



# A Sensitive and Selective Electrochemical Aptasensor Based On Gold Nanoflower/Polyethyleneimine (Pei)-Functionalized Metal Organic Framework Nanocomposites for Label-Free Determination of Streptomycin in Milk Samples

Yuanyuan Hui<sup>1</sup> · Haishuai Peng<sup>1</sup> · Linqiang Li<sup>1</sup> · Aiqing Zhao<sup>1</sup> · Ding Yang<sup>1</sup> · Weizhe Wang<sup>1</sup> · Bini Wang<sup>1,2</sup>

Received: 17 September 2022 / Accepted: 10 January 2023 / Published online: 19 January 2023  
© The Author(s), under exclusive licence to Springer Science+Business Media, LLC, part of Springer Nature 2023

## Abstract

Rapid, accurate, sensitive, and real-time detection of streptomycin (STR) residues in dairy products is very important. In this work, for the first time, the gold nanoflower/polyethyleneimine-functionalized metal organic framework (AuNF-PEI-MIL-101(Cr)) nanocomposites were synthesized via hydrothermal method and characterized using various techniques (SEM, TEM, XRD, FT-IR, and XPS). Then, a novel electrochemical aptasensor was constructed for the detection of STR based on AuNF-PEI-MIL-101(Cr) nanocomposites. The gold electrode (GE) modified with AuNF-PEI-MIL-101(Cr) can immobilize a large number of thiolated STR aptamer via the Au–S bond. When the target STR was in the presence, the current signal was reduced due to the specific binding of STR towards the aptamer. The results indicated that the aptasensor had a wide linear range towards STR (0.01–400 nM) with a low detection limit of 0.003 nM under the optimal conditions. Moreover, the aptasensor exhibited good selectivity, reproducibility, and stability. In addition, the STR in the cow, sheep, and goat milk samples was detected by the spiked recovery method, and satisfactory results were obtained. The method provides an efficient pathway for the sensitive detection of STR.

**Keywords** Electrochemical sensing · Aptasensor · Antibiotics · Metal–organic framework · Polyethyleneimine · Gold nanoflower

## Introduction

With the improvement of living standards, there is a gradual increase in consumer demand for milk and other dairy products. In order to reduce the economic losses of the breeder

and ensure milk production volume, streptomycin (STR), an aminoglycoside antibiotic, is often added to animal feed to prevent and treat mastitis, a disease caused by gram-negative bacteria and *Mycobacterium tuberculosis* (Zhang et al. 2018a, b). However, the excessive use and abuse of streptomycin leads to antibiotic residues in milk that cause serious side effects on consumers, such as ototoxicity and nephrotoxicity (Meng et al. 2020). Thus, to effectively monitor streptomycin residues and protect human health, regulatory authorities have established maximum residue limits (MRLs) for streptomycin in food. The European Union has regulated the maximum residue limit for streptomycin in milk at 200  $\mu\text{g kg}^{-1}$ , and similar regulations have been presented in other countries (European Commission. 2010). Thus, the detection of streptomycin in milk and dairy products has vital significance.

Currently, high-performance liquid chromatography (HPLC) (Chen et al. 2012), liquid chromatography-mass spectrometry (LC–MS) (Kaufmann et al. 2012; Vanbruijnsvoort et al. 2004), and enzyme-linked immunosorbent

## Highlights

1. The presence of AuNF-PEI-MIL-101(Cr) on the sensor surface increases the aptamer loading efficiency.
2. The developed aptasensor exhibits wide linear range and low detection limit for streptomycin.
3. The aptasensor shows high sensitivity and selectivity.
4. Fabricated aptasensor can be proposed for monitoring other antibiotics in foodstuffs.

✉ Bini Wang  
biniwang@snnu.edu.cn

<sup>1</sup> College of Food Engineering and Nutritional Science, Shaanxi Normal University, Xi'an 710119, Shaanxi, China

<sup>2</sup> Shaanxi Provincial Key Laboratory of Electroanalytical Chemistry, Northwest University, Xi'an 710069, Shaanxi, China

assay (ELISA) (Ho et al. 2013) are the most commonly used methods for the detection of streptomycin. Despite having low detection limits and high accuracy and precision, these methods still suffer from many limitations, such as being complex, time-consuming, labor-intensive, and instrument-expensive. Therefore, the design of a fast, sensitive, and economic method for the detection of STR has become a research hotspot. Electrochemical aptasensors are a type of small analytical device in which an aptamer serves as a recognition element and exhibit great promise in detecting STR because of their low cost, rapid response, and high sensitivity.

To improve the analytical performance of electrochemical aptasensors, electrodes are usually modified with suitable nanomaterials. At present, various kinds of nanomaterials have been applied to construct electrochemical aptasensors, such as carbon nanotubes (CNTs) (Thakur et al. 2017), graphene oxide (GO) (Gzde and Pekyardmc 2020), carbon dots (CDs) (Huang et al. 2022), metal nanoparticles (NPs) (Vilalanga et al. 2022), covalent organic frameworks (COFs) (Zhu et al. 2021), and metal–organic frameworks (MOFs) (Duan et al. 2019). Among these, MOFs are novel porous materials composed of metal ions and organic ligands through coordination bonds (Mehmandoust et al. 2023). Owing to their high surface area, large porosities, and tunable framework, MOFs have been applied in various fields, including gas storage and separation (Hai and Wang 2022), catalysis (Cheng et al. 2018), drug delivery (Suresh and Matzger 2019), adsorption (Yuan et al. 2021), and sensing (Mehmandoust et al. 2022). However, because of the poor electrical conductivity and stability, the applications of many traditional MOFs are greatly limited. To enhance the electrical conductivity without destroying the pristine structure, they could be modified with functional groups such as  $-\text{NH}_2$  and  $-\text{OH}$ , which improved the stability and electron transfer ability of MOFs while also supplying more binding sites for the recognition of biomolecules like antibodies, DNA, and aptamers. Polyethylene (PEI) is a water-soluble polymer with a high density of amine groups that has been widely used for biological applications and has strong adsorption for heavy metal ions via chelation (Zhao et al. 2016). Inspired by this, PEI-functionalized MOF (PEI-MOF) nanocomposite was designed and prepared. Compared with pure MOFs, PEI-functionalized MOFs (PEI-MOFs) have good dispersibility and electroconductivity (Chen et al. 2019; He and Wang 2021). Another an effective and feasible strategy for improving the electrochemical properties of MOFs is to combine them with conductive and stable materials (such as carbon-based materials, metal nanoparticles, and noble metal) to form composites. For example, Lu et al. designed graphene aerogel/metal–organic framework (GA/UiO-66- $\text{NH}_2$ ) nanocomposites via a facile hydrothermal method and applied them for the detection of multiple heavy-metals.

The large specific surface area and hierarchical porous structure of the GA/UiO-66- $\text{NH}_2$  composites were beneficial for electron transfer (Lu et al. 2018). Biswas et al. successfully synthesized Zr-trimesic acid MOF/carbon nanotube (MOF-808/CNT) nanocomposites through an in situ formation of MOF-808 on the activated CNT and used them as a sensing platform to fabricate a label-free electrochemical immunosensor for detection of the ovarian cancer biomarker, carbohydrate antigen 125 (CA 125) (Biswas et al. 2021). Wang et al. prepared AuNPs/metal-metalloporphyrin frameworks (AuNPs/MMPF-6(Fe)) nanocomposites using the principle of electrostatic adsorption. Due to the strong synergistic catalysis effects, enlarged active surface area, and high conductivity, the AuNPs/MMPF-6(Fe) composite could ultra-sensitively detect hydroxylamine (Wang et al. 2016). Considering the large specific surface area, high surface free energy, and good conductivity and biocompatibility of flower-like gold nanoparticles (AuNF), the combination of PEI-MOFs and AuNF not only improved the electron transfer ability of MOFs, but also provided more catalytic sites. Besides, AuNF adsorbing on the surface or surface pores of MOF can prevent the aggregation of AuNF because of the support effect or restriction effect (Sun et al. 2022). Therefore, combining AuNF with PEI-MOFs is expected to be an excellent electrode-modified material.

In this work, the AuNF-PEI-MIL-101(Cr) nanocomposites were synthesized via hydrothermal method, and their morphology, structure, size, and composition were characterized by SEM, TEM, XRD, FT-IR, and XPS analysis techniques. Then, a simple and sensitive electrochemical aptasensor based on AuNF-PEI-MIL-101(Cr) nanocomposite was fabricated for the determination of STR. The bare gold electrode (GE) was modified with AuNF-PEI-MIL-101(Cr) by weak covalent bonding and electrostatic interactions. The aptamer of STR was immobilized onto AuNF-PEI-MIL-101(Cr) via Au–S bond and electrostatic interactions. The specific binding of STR to its aptamer results in the conformational change of aptamer strands and the decrease of current signal in the presence of the target STR. The larger the STR concentrations, the weaker the current signal. The designed electrochemical aptasensor is a promising platform for the detection of STR in dairy products.

## Materials and Methods

### Materials

The thiolated STR aptamer was synthesized by Shanghai Biotechnology Co., Ltd., and the oligonucleotide sequences are as follows: 5'-HS-( $\text{CH}_2$ )<sub>6</sub>-TAG GGA ATT CGT CGA CGG ATC CGG GGT CTG GTG TTC TGC TTT GTT CTG

TCG GGT CGT CTG CAG GTC GAC GCA TGC GCC G-3'. The dissociation constant ( $K_d$ ) of the STR aptamer is 199.1 nM (Zhou et al. 2013).

Streptomycin was purchased from Shanghai Macklin Biochemical Co., Ltd. (Shanghai, China).  $\text{Cr}(\text{NO}_3)_3 \cdot 9\text{H}_2\text{O}$  (99.0%), N, N-dimethylformamide (DMF, 99.5%), terephthalic acid hydrofluoric acid (HF, 40%), polyethyleneimine (PEI, Branched, and M.W. 70,000, 50% W/V aqueous solution), potassium hexacyanoferrate (II) trihydrate ( $\text{K}_4[\text{Fe}(\text{CN})_6] \cdot 3\text{H}_2\text{O}$ , 99.0%), potassium hexacyanoferrate (III) ( $\text{K}_3[\text{Fe}(\text{CN})_6]$ , 99.0%), chloride trihydrate ( $\text{HAuCl}_4 \cdot 3\text{H}_2\text{O}$ ,  $\geq 99.9\%$ ), trisodium citrate, and hydroquinone were purchased from Aladdin Chemistry Co., Ltd. (Shanghai, China). STR ELISA kits were purchased from Shanghai Enzyme-linked Biotechnology Co., Ltd (Shanghai, China). The water used in all experiments was ultrapure water, which was purified by a Milli-Q Water System ( $\geq 18 \text{ M}\Omega$ ).

## Apparatus

The nanomaterials were characterized by the scanning electron microscope (SEM, SU8220, Hitachi, Japan), transmission electron microscope (TEM, JEOL JEM-2800, Japan), X-ray powder diffraction (XRD, Smart Lab (9), Rigaku Corporation, Japan), Fourier transform infrared spectrum (FT-IR, Tensor27, Bruker, Germany), and X-ray photoelectron spectroscopy (XPS, ESCALAB Xi+, Thermo Fisher Scientific, USA).

Electrochemical measurements were carried out with a CHI 660E electrochemical workstation (CH Instruments, Shanghai, China). A three-electrode system was composed of a gold electrode (GE) as the working electrode, Ag/AgCl as the reference electrode, and platinum wire as the counter electrode. Cyclic voltammetry (CV) and electrochemical impedance spectroscopy (EIS) were used to characterize the aptasensor fabrication process in 5 mM  $[\text{Fe}(\text{CN})_6]^{3-/4-}$  solution containing 0.1 M KCl. CV curves were recorded from  $-0.2 \text{ V}$  to  $0.6 \text{ V}$  at a scan rate of  $0.05 \text{ V s}^{-1}$ . EIS dates were performed in the frequency range of 10 kHz to 0.1 Hz with a signal amplitude of 10 mV. Differential pulse voltammetry (DPV) was measured in 0.1 M PBS containing 5 mM  $[\text{Fe}(\text{CN})_6]^{3-/4-}$  and 0.1 M KCl with a potential range from  $-0.2 \text{ V}$  to  $0.6 \text{ V}$  at 50 mV pulse amplitude, 0.05 pulse width and 0.5-s pulse period.

## Synthesis of AuNF

AuNF was prepared according to the seed-mediated growth method (Zhou et al. 2017). Firstly, colloidal gold seed solutions were synthesized through classical hydrothermal reduction with citrate. Briefly, 100 mL of 0.01%  $\text{HAuCl}_4$  were brought to a boil with vigorous stirring. Subsequently,

3 mL of 1% (w/v) trisodium citrate was added rapidly to the solution. When the color changed from pale yellow to wine red, the mixture was heated for another 15 min. The obtained colloidal gold seed solutions were cooled to room temperature for subsequent use. Then, 2.7 mL of colloidal gold seed solutions, 1.2 mL of 1% (w/v)  $\text{HAuCl}_4$ , and 2.7 mL of 1% (w/v) trisodium citrate were added to 100 mL of ultrapure water ( $50^\circ\text{C}$ ). After 15 s, 24.0 mL of 30 mM hydroquinone was rapidly added into this mixture and stirred for 30 min at room temperature. The resulting AuNF was stored at  $4^\circ\text{C}$  for further use.

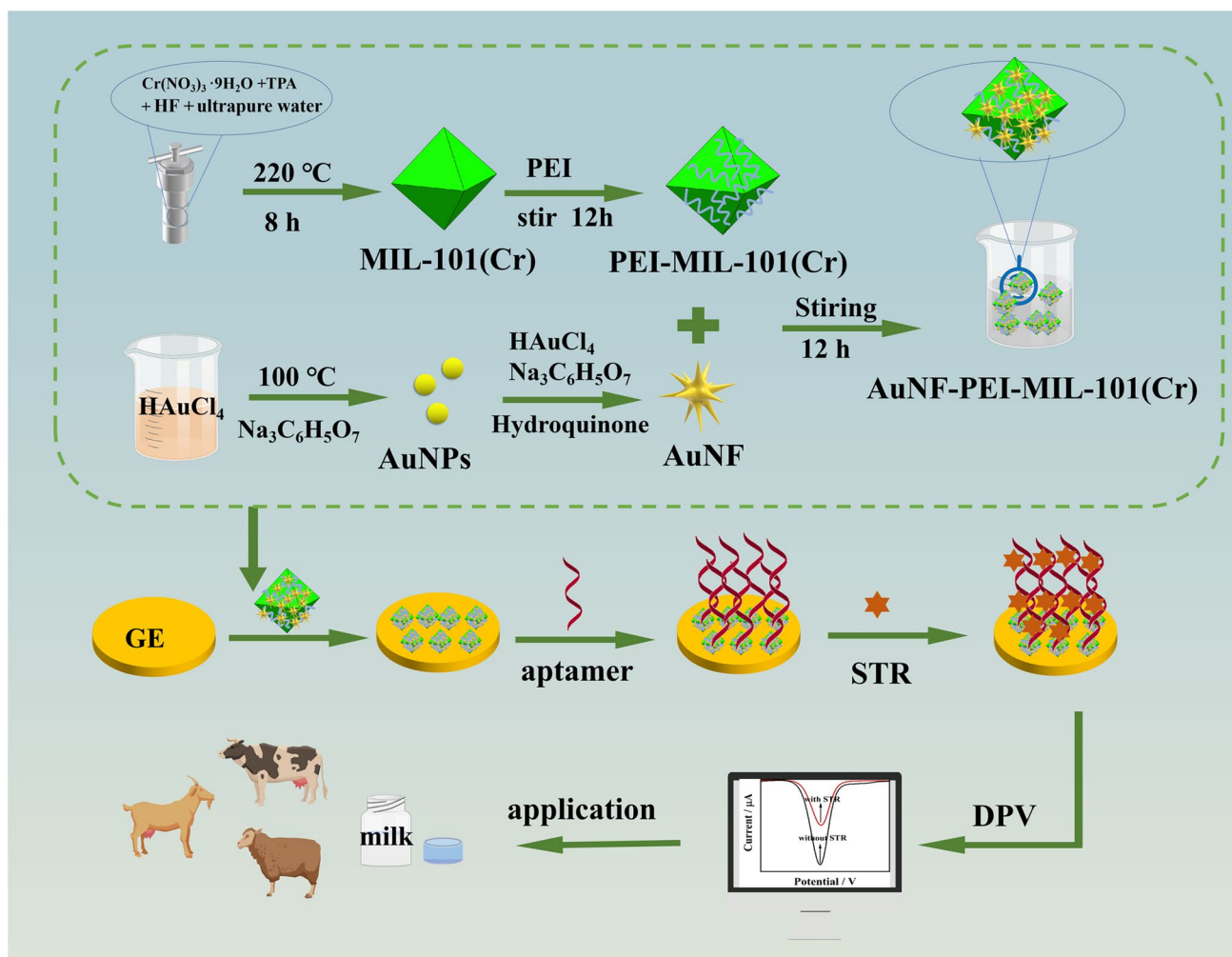
## Synthesis of AuNF-PEI-MIL-101(Cr)

MIL-101(Cr) was prepared according to the method described in the literature (Yao et al. 2021). Firstly, 2.4 g 1.0  $\text{Cr}(\text{NO}_3)_3 \cdot 9\text{H}_2\text{O}$ , 996 mg TPA, and 1.2 mL HF (6.0 mmol) were added to 30 mL ultrapure water and stirred for 30 min. Then, the mixture solution was transferred to a 100-mL Teflon-lined stainless steel autoclave and heated at  $220^\circ\text{C}$  for 12 h. After cooling down to room temperature, the mixture was centrifuged for 15 min at 10,000 rpm, followed by washed three times with DMF (N, N-dimethylformamide) and anhydrous ethanol. Finally, the solid was vacuum dried at  $40^\circ\text{C}$ . The obtained MIL-101(Cr) was stored in a desiccator for future use.

The PEI-MIL-101(Cr) nanomaterials were synthesized according to the previous report (Yao et al. 2021). In brief, 5 mL of PEI (1 wt %) was mixed with 10 mL of MIL-101(Cr) solution ( $1 \text{ mg mL}^{-1}$ ) with mild stirring for over 12 h. After centrifugation, the green product was washed with deionized water several times, and the resultant product was re-dispersed in 5 mL of ultrapure water. Next, 2 mL of PEI-MIL-101(Cr) was added to the 20 mL of AuNF, and the mixture was stirred at room temperature for 12 h. Finally, the obtained AuNF-PEI-MIL-101(Cr) was washed with ultrapure water and then dried at  $65^\circ\text{C}$  for 24 h.

## Construction of the Aptasensor

The bare gold electrode (GE) was first pretreated in freshly prepared piranha solution (the volume ratio of 98%  $\text{H}_2\text{SO}_4$  to 30%  $\text{H}_2\text{O}_2$  equals 7:3) for 5 min, and polished carefully with  $0.05 \mu\text{m}$   $\text{Al}_2\text{O}_3$  powder, and then ultrasonically cleaned with deionized water for 5 min. Subsequently, GE was electrochemically cleaned in a 0.5 M  $\text{H}_2\text{SO}_4$  solution for 10 min by CV scanning ( $-0.2 \text{ V}$ - $0.6 \text{ V}$ ) until a stable CV curve was achieved and rinsed out thoroughly with ultrapure water. Afterwards, 10  $\mu\text{L}$  of AuNF-PEI-MIL-101(Cr) nanocomposites were dripped on the GE surface. After drying at room temperature and washing with ultrapure water, 10  $\mu\text{L}$  of thiolated aptamer solution (2  $\mu\text{M}$ ) was dripped to the surface of AuNF-PEI-MIL-101(Cr)/GE via Au-S bond. Then the



**Scheme 1** Schematic of the fabrication of the electrochemical aptasensor

aptamer/AuNF-PEI-MIL-101(Cr)/GE was incubated with different concentrations of STR for 2 h at room temperature. The electrochemical signals of the STR/aptamer/AuNF-PEI-MIL-101(Cr)/GE were measured using DPV. For each step, the modified electrodes were gently rinsed with ultrapure water. The detailed fabrication procedure is shown in Scheme 1.

### Samples Preparation

The cow milk was purchased from Vanguard supermarket (Shaanxi, China). The sheep milk and goat milk were obtained from Gansu Yuansheng Agriculture and Animal Husbandry Technology Co., Ltd. (Gansu, China), and Xi'an Baiyue Goat Milk Group Co., Ltd. (Shaanxi, China), respectively. They were treated according to the literature reported by our group previously (Hui et al. 2022). Firstly, 25 mL of milk samples were placed in a water bath (65 °C) for 30 min, followed by centrifugation at 20,000 rpm for 30 min. Three distinct phases were present in the centrifuge

tube. The upper fat layer was discarded, and the middle aqueous phase was carefully recovered. Then, the recovered liquid was filtrated with a sterile Millipore membrane (0.22 μm). Finally, the 0.2 mL of the filtered supernatant was diluted 10 folds with Tris buffer solution and spiked with different concentrations of STR for spiked recovery experiments. Furthermore, the ELISA method was performed to verify the developed aptasensor according to the Chinese National Standard (GB/T 21,330–2007).

### Results and Discussion

#### Principles of STR Detection by the Aptamer/AuNF-PEI-MIL-101(Cr)/GE

The working principle of the label-free electrochemical aptasensor is illustrated in Scheme 1. The bare GE surface was first modified by AuNF-PEI-MIL-101(Cr)

nanomaterials. Then, the aptamer was self-assembled on the AuNF-PEI-MIL-101(Cr)/GE via electrostatic adsorption and Au–S bond. Upon introducing the STR, specific binding was performed based on the high recognition ability between the aptamer and the STR. At the same time, the combination of STR and aptamer created steric hindrance, making it difficult for  $[\text{Fe}(\text{CN})_6]^{3-/4-}$  anions to reach the sensing interface, and thereby reducing current signals. As a result, the concentration of target STR can be determined based on the change in current signal caused by the specific recognition and binding via DPV measurements.

### Morphology, Structure, Composition, and Size of Nanomaterials

SEM and TEM are used to investigate the surface morphology, microstructure, and size of these nanomaterials. As shown in Fig. 1A and B, the MIL-101(Cr) has a relatively smooth surface and an octahedral morphology with a size of about 500–600 nm. After MIL-101(Cr) functionalization with PEI (Fig. 1C, D), PEI-MIL-101(Cr) did not undergo any significant size or morphology change. Figure 1E shows the TEM image of the AuNF, which exhibits a flower-like structure with a uniform particle size and a diameter of about 50 nm.

Figure 1F and G depict the TEM and SEM of AuNF-PEI-MIL-101(Cr). It can be observed that AuNF was successfully loaded on the surface of PEI-MIL-101(Cr). In addition, the elemental composition of the AuNF-PEI-MIL-101(Cr) nanocomposites was further investigated by high-angle annular dark-field scanning transmission electron microscopy (HAADF-STEM). As shown in Fig. 1H and J, the Au element is located on the outside of the Cr element, indicating the successful synthesis of the AuNF-PEI/MIL-101(Cr) nanohybrid.

Powder X-ray diffraction (XRD) is employed to characterize the crystalline structure of nanomaterials. The XRD patterns of MIL-101(Cr), PEI-MIL-101(Cr), and AuNF-PEI-MIL-101(Cr) are shown in Fig. 2A. MIL-101(Cr) showed diffraction peaks at  $2\theta$  of  $5.56^\circ$ ,  $8.98^\circ$ ,  $16.42^\circ$ , and  $24.72^\circ$  (black line), which were consistent with previous literature (Pourreza et al. 2019). After being functionalized by PEI (red line), PEI-MIL-101(Cr) exhibited similar diffraction peaks to MIL-101(Cr), indicating the crystal structure has not changed. While the intensity of diffraction peaks were reduced. This was attributed to the filling of MIL-101(Cr) pores by PEI, which decorated the pore properties, such as pore size and polarity (Xin et al. 2015). In addition, the AuNF-PEI-MIL-101(Cr) not only showed all the diffraction peaks of the PEI-MIL-101(Cr), but also four additional diffraction peaks at  $38.06^\circ$ ,  $44.18^\circ$ ,

**Fig. 1** A SEM and B TEM images of MIL-101(Cr); C SEM and D TEM images of PEI-MIL-101(Cr); E TEM images of AuNF; F SEM and G TEM images of AuNF-PEI-MIL-101(Cr); H–J HAADF-STEM element mapping images of AuNF-PEI-MIL-101(Cr)

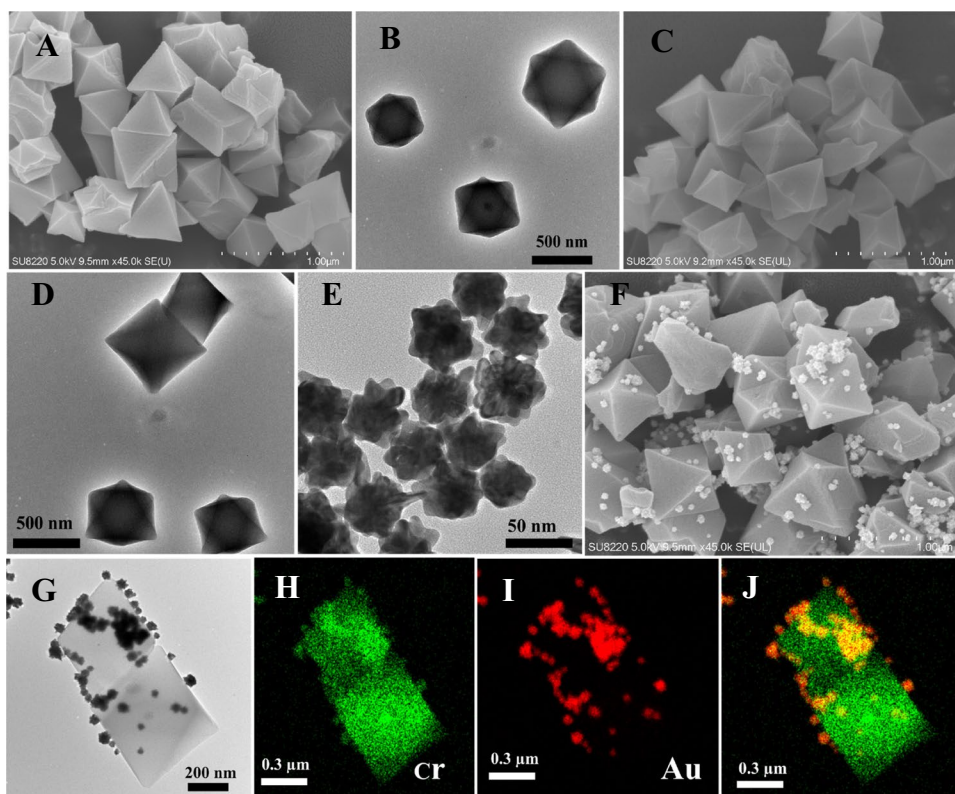
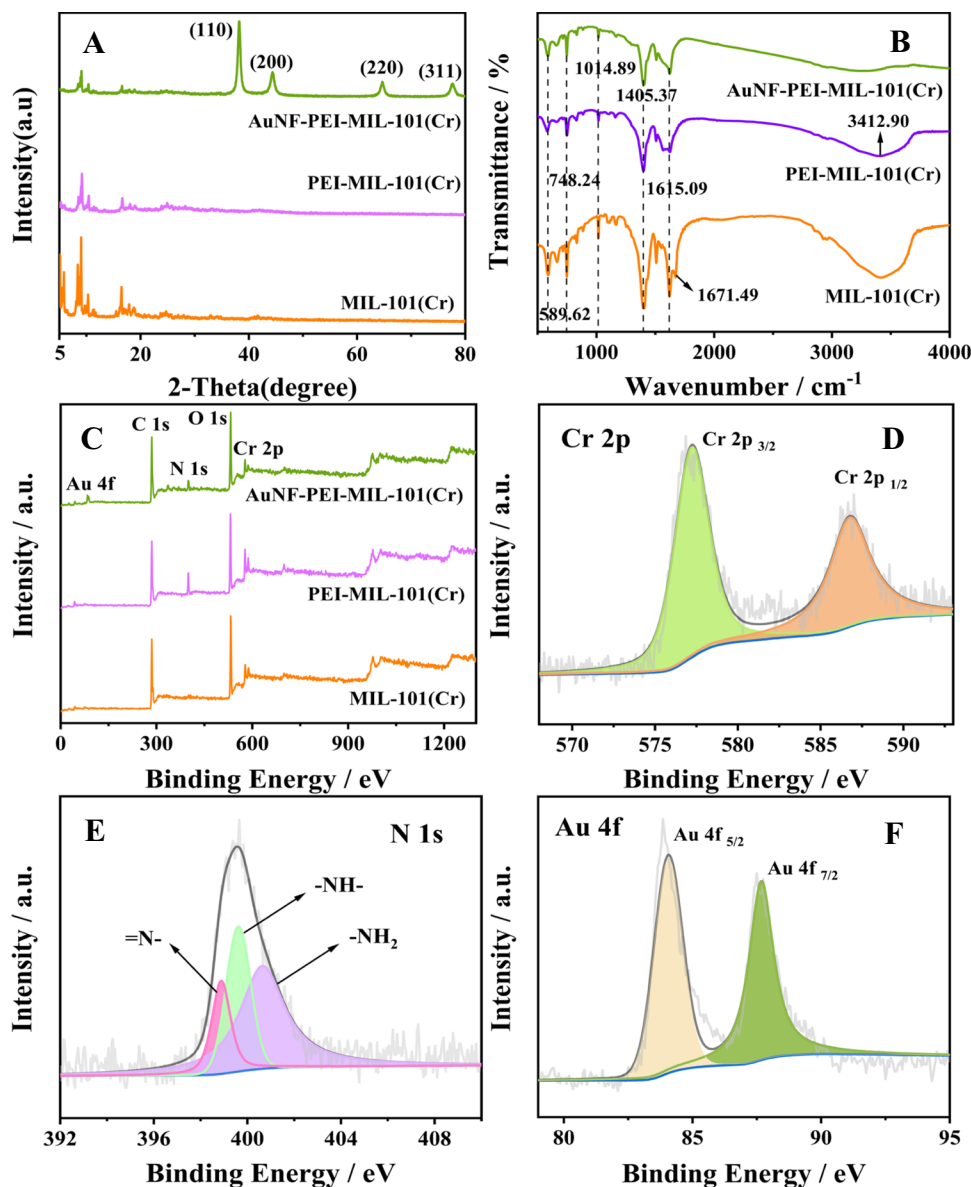


**Fig. 2** A XRD patterns of MIL-101(Cr), PEI-MIL-101(Cr), and AuNF-PEI-MIL-101(Cr); B FT-IR spectra of MIL-101(Cr), PEI-MIL-101(Cr), and AuNF/PEI-MIL-101(Cr); C XPS spectra of AuNF/PEI-MIL-101(Cr); High-resolution XPS spectra of Cr2p (D), Au4f (E), and C1s (F) in AuNF/PEI-MIL-101(Cr)



64.64, and 77.42, corresponding to (111), (200), (220), and (311) faces of Au (Lu et al. 2014).

FT-IR is used to identify the functional groups in MIL-101(Cr), PEI-MIL-101(Cr), and AuNF-PEI-MIL-101(Cr). As shown in Fig. 2B, the FTIR spectrum of MIL-101(Cr) displayed obvious vibration peaks at 589.62, 748.24, 1014.89, 1405.37, 1615.09, and 3340.10  $\text{cm}^{-1}$ . The peak at 589.62  $\text{cm}^{-1}$  belonged to the vibration of Cr–O bond (Bayazit et al. 2017), and the vibration peak at 748.24  $\text{cm}^{-1}$  assigned to the deviational vibration of carboxylate groups. At 1014.89  $\text{cm}^{-1}$ , in-plane bending vibration of C–H on the benzene ring was observed. The two peaks at 1405.37  $\text{cm}^{-1}$  and 1615.09  $\text{cm}^{-1}$  may be due to both the symmetric stretching and asymmetric tensile vibration of the carboxyl ( $-\text{COO}^-$ ) group, respectively (Wan et al. 2021; Zhang et al. 2021). After modification of MIL-101(Cr) with

PEI, the spectrum of the PEI-MIL-101(Cr) exhibited some changes. The peak at 1671.98  $\text{cm}^{-1}$  disappeared. The peak at 3412.90  $\text{cm}^{-1}$  can be attributed to N–H bond in the secondary amine group, indicating that the PEI had been successfully grafted onto the MIL-101(Cr) (Wan et al. 2021). However, compared with PEI-MIL-101(Cr), the absorption peak shape and peak intensity of AuNF-PEI-MIL-101(Cr) are changed (decreased or increased), indicating the composition of hybrid AuNF-PEI-MIL-101(Cr).

X-ray photoelectron spectroscopy (XPS) is employed to analyze the chemical states and elemental composition of AuNF-PEI-MIL-101(Cr). Figure 2C shows the XPS survey spectrum of the AuNF-PEI-MIL-101(Cr) nanocomposites, in which the characteristic peaks of N 1s, Cr 2p, and Au 4f could be all clearly observed. For the high-resolution Cr 2p spectrum (Fig. 2D), the two peaks at

577.25 eV and 586.75 eV can be assigned to Cr 2p<sub>3/2</sub> and Cr 2p<sub>1/2</sub>, revealing the existence of Cr–O bond (Cheng et al. 2020). The high-resolution N 1s spectrum (Fig. 2E) can be divided into three peaks. The main peak at 399.8 eV is attributed to secondary amine (–NH–), and the peaks at 398.89 eV and 400.64 eV belong to tertiary (–N–) and primary (–NH<sub>2</sub>) amine groups, respectively (Shen et al. 2021). These nitrogen species are typical chemical compositions of PEI, indicating that PEI has been successfully modified to the surface of MIL-101(Cr). The high-resolution Au 4f spectrum (Fig. 2F) exhibits two peaks at 84.05 eV and 87.65 eV which were assigned to the Au 4f<sub>7/2</sub> and the Au 4f<sub>5/2</sub>, respectively, proving the Au (0) is present in AuNF-PEI-MIL-101(Cr). These experimental results well demonstrated that AuNF-PEI-MIL-101(Cr) nanocomposites were successfully synthesized.

### Electrochemical Behavior of AuNF-PEI-MIL-101(Cr)/GE

The CV curves of bare GE and AuNF-PEI-MIL-101(Cr)-modified GE at different scan rates (20–100 mV s<sup>-1</sup>) are shown in Fig. 3A and B. Both bare GE and AuNF-PEI-MIL-101(Cr)/GE showed a pair of well-defined redox peaks. Figure 3C and D show the relationship between the redox peak current (*I*<sub>pa</sub>/*I*<sub>pc</sub>) versus the square root of the scan rate (*v*<sup>1/2</sup>). It is observed that *I*<sub>pa</sub> and *I*<sub>pc</sub> are linearly proportional to *v*<sup>1/2</sup> in the range of 20–100 mV s<sup>-1</sup>, suggesting that a diffusion controlled process occurred on the bare GE and AuNF-PEI-MIL-101(Cr)/GE. Thus, the electrochemically active surface area (EASA) was calculated according to the modified-quasi-reversible Randles–Ševčík (RS) equation (De Carvalho et al. 2020).

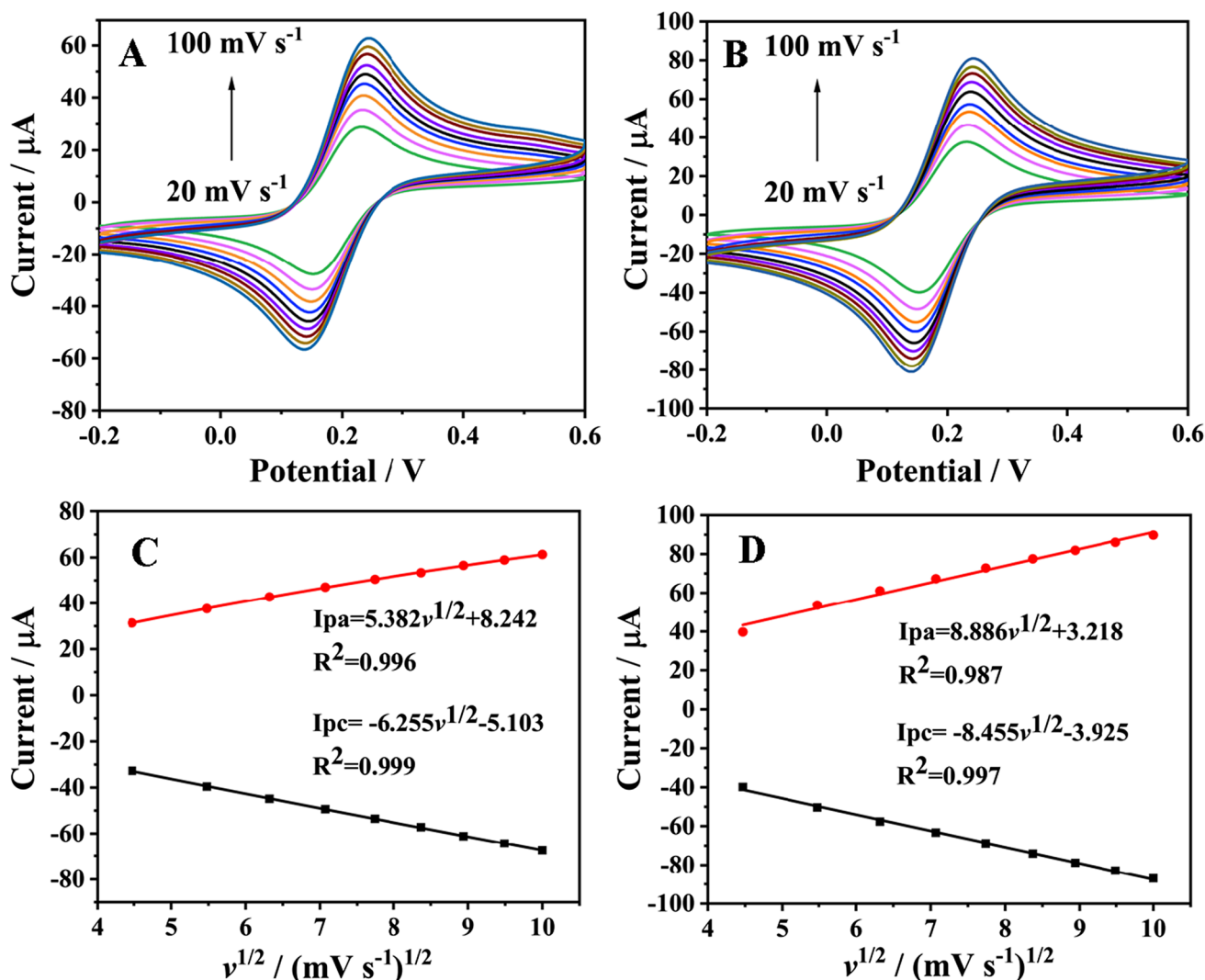


**Fig. 3** CV curves of **A** GE and **B** AuNF-PEI-MIL-101(Cr)/GE at various scan rates (20, 30, 40, 50, 60, 70, 80, 90, 100 mV s<sup>-1</sup>). The linear relationship between the redox peak current *I*<sub>p</sub> and square root of the scan rate (*v*<sup>1/2</sup>) of **C** GE and **D** AuNF-PEI-MIL-101(Cr)/GE

$$I_p = 2.99 \times 10^5 AD^{1/2} a^{1/2} n^{3/2} \nu^{1/2} C \quad (1)$$

In the formula,  $I_p$  is the peak current ( $\mu\text{A}$ ),  $A$  is the electroactive surface area ( $\text{cm}^2$ ),  $D$  is the diffusion coefficient of  $[\text{Fe}(\text{CN})_6]^{3-/4-}$  ( $D = 6.3 \times 10^{-6} \text{ cm}^2 \text{ s}^{-1}$ ),  $\alpha$  is the transfer coefficient (usually taken to be close to 0.5),  $n$  is the number of transfer electrons ( $n = 1$  for  $[\text{Fe}(\text{CN})_6]^{3-/4-}$ ),  $\nu$  is the scan rate ( $\text{V s}^{-1}$ ), and  $C$  is the redox medium concentration ( $C = 5.0 \text{ mol cm}^{-3}$ ). The EASA of the bare GE and AuNF-PEI-MIL-101(Cr)/GE were  $0.0402 \text{ cm}^2$  and  $0.0522 \text{ cm}^2$ , respectively. The AuNF-PEI-MIL-101(Cr)/GE was 1.30 times that of the bare GE, demonstrating AuNF-PEI-MIL-101(Cr)/GE has a faster electron transfer rate.

### Electrochemical Characterization of the Stepwise Modification Process

The EIS measurements were carried out during the construction process of the electrochemical aptasensor using  $[\text{Fe}(\text{CN})_6]^{3-/4-}$  as a redox probe. In the EIS spectrum, the semicircle diameter equals the electron transfer resistance ( $R_{et}$ ). As shown in Fig. 4A, the bare GE possessed a low electron transfer resistance (curve a), indicating superior conductive property. When the AuNF-PEI-MIL-101(Cr) was modified on the surface of GE, the  $R_{et}$  decreased because the nanocomposites accelerated the electron transfer of  $[\text{Fe}(\text{CN})_6]^{3-/4-}$  on the GE surface (curve b). However, with the immobilization of thiolated Apts on the AuNF-PEI-MIL-101(Cr)/GE via Au–S bond, the  $R_{et}$  increased (curve c). This is because negatively charged phosphate backbone of the aptamer made  $[\text{Fe}(\text{CN})_6]^{3-/4-}$  anions inaccessible to the electrode surface. In the presence

of STR, a decrease in  $R_{et}$  is observed, which is caused by the target being specifically bound with the aptamer on the surface of the aptamer/AuNF-PEI-MIL-101(Cr)/GE.

CV is another effective approach used to monitor the aptasensor assembly. As shown in Fig. 4B, the bare GE exhibited clearly separated redox peaks of  $[\text{Fe}(\text{CN})_6]^{3-/4-}$  in the range of  $-0.2 \text{ V}$ – $0.6 \text{ V}$  (curve a'). When AuNF-PEI-MIL-101(Cr) were modified onto the GE, the peak current was obviously increased relative to the bare GE. This change is attributed to the good conductivity of AuNF-PEI-MIL-101(Cr) (curve b'). After the STR aptamer immobilization onto the AuNF-PEI-MIL-101(Cr)/GE, the current signal significantly diminished (curve c'). When the STR appeared, the current signal further decreased (curve d'), suggesting that the formation of the aptamer-STR complex hindered the interfacial electron transfer to the modified electrode surface. The CV results were in accordance with EIS. These results greatly demonstrate that the electrochemical aptasensor was successfully constructed.

### Optimization of the Electrochemical Sensing Conditions

In order to achieve the best analytical performance of the aptasensor, the experimental conditions were optimized, namely the concentration of aptamer, the incubation time of aptamer, and the incubation time of STR.

To investigate the effect of the aptamer concentration on the changes in the current response ( $\Delta I = I - I_0$ , where  $I$  is the current signal of the aptasensor toward STR, and  $I_0$  is the background signal), aptamer with different concentrations ( $0.5, 1.0, 1.5, 2.0, 2.5,$  and  $3.0 \mu\text{M}$ ) were fixed to the

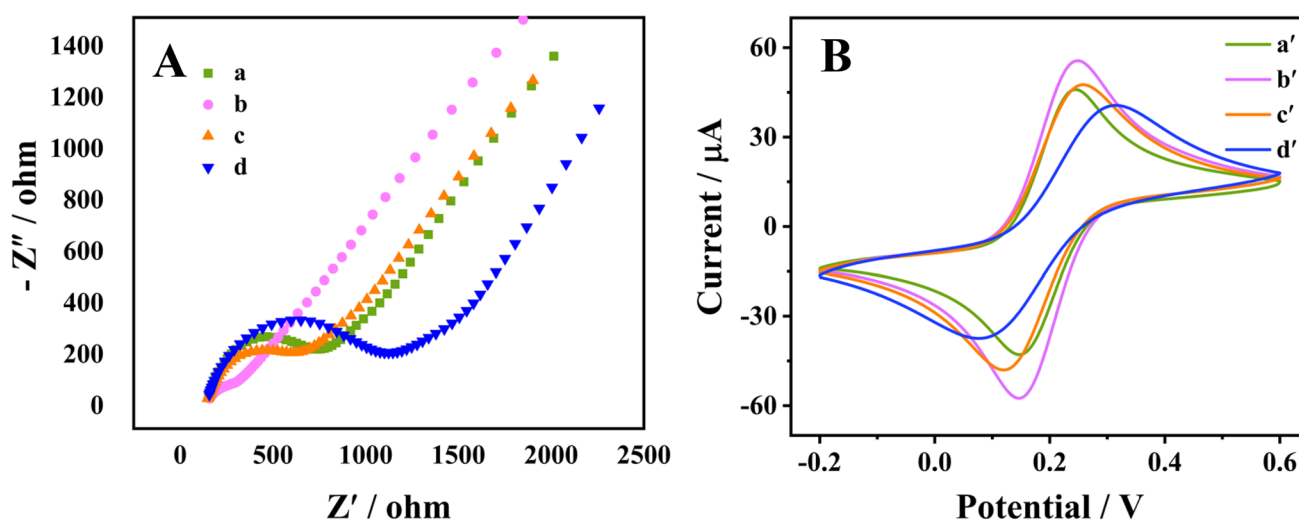


**Fig. 4** **A** EIS and **B** CV characterization of the construction process of electrochemical aptasensor. (a,a') GE, (b,b') AuNF-PEI-MIL-101(Cr)/GE, (c,c') aptamer/AuNF-PEI-MIL-101(Cr)/GE, (d,d') STR/aptamer/AuNF-PEI-MIL-101(Cr)/GE. The concentration of STR was  $50 \text{ nM}$



surface of the modified electrode during the construction of the aptasensor and the current signals were recorded. As shown in Fig. S1A, the  $\Delta I$  (the difference between the DPV peak current in the presence of the STR and that of the blank) increased gradually with the increase of aptamer concentration from 0.5 to 2.0  $\mu\text{M}$ , and then remained almost constant, indicating that the aptamer was saturated at the electrode surface. Therefore, 2.0  $\mu\text{M}$  was selected as the optimum concentration of aptamer in subsequent experimental assays.

The aptamer incubation time is an essential factor affecting the performance of the aptasensor. If the incubation time of the aptamer is too short, the aptamer will not be completely immobilized on the AuNF-PEI-MIL-101(Cr)/GE. Vice versa, this process may take too much time. The working electrodes were separately placed in 2.0  $\mu\text{M}$  of aptamer solution for different times (40, 50, 60, 70, 80, and 90 min). As shown in Fig. S1B, with increasing incubation times from 40 to 60 min, the  $\Delta I$  increases. When the incubation time was greater than 60 min, there was no obvious change in the  $\Delta I$ . Thus, 60 min was selected as the best aptamer incubation time for the aptamer/AuNF-PEI-MIL-101(Cr)/GE.

The incubation time of STR with the aptamer was also investigated. The aptamer/AuNF-PEI-MIL-101(Cr)/GE was separately incubated with the STR (200 nM) for different times (40, 50, 60, 70, 80, and 90 min). As shown in Fig. S1C, the maximum  $\Delta I$  was obtained at 60 min of incubation time, but it subsequently exhibited a downward trend. Hence, 60 min was selected as the optimal incubation time for STR.

## Analytical Performance of the Electrochemical Sensing Method

Under the optimal experimental conditions, the aptamer/AuNF-PEI-MIL-101(Cr)/GEs were placed in different concentrations of STR (0.01 nM, 0.1 nM, 1 nM, 10 nM, 50 nM, 100 nM, 150 nM, 200 nM, 250 nM, 300 nM, 350 nM, 400 nM), and their DPV peaks current were recorded. As shown in Fig. 5A, the signals decreased with increasing the STR concentration within the range of 0.1–400 nM. Figure 5B exhibited the linear relationship between the current response difference ( $\Delta I$ ) and STR concentrations ( $\Delta I = I - I_0$ , where  $I$  is the current signal of the aptasensor toward STR, and  $I_0$  is the background signal). The linear equation was  $\Delta I = 0.124 C_{\text{STR}} + 0.9955$  ( $R^2 = 0.9988$ ), and the limit of detection (LOD) was calculated to be 0.003 nM based on  $3S/N$  (where  $S$  is the standard deviation of blank samples and  $N$  is the slope of the calibration plot). Compared with previously reported methods for detection of STR (Table S1) (Chen et al. 2012; Luo et al. 2020; Taghdisi et al. 2016; Xu et al. 2017; Yin et al. 2017), the developed electrochemical aptasensor had a wider detection range and a lower detection limit. Moreover, the maximum residue limits (MRLs) of STR for milk were 200  $\mu\text{g kg}^{-1}$  stipulated by the European Union (EU). It is obvious that the detection limits of the developed aptasensor are much lower than those of these regulation level. Importantly, whole detection could be completed within 60 min. These excellent performances could be attributed to the following two aspects: (i) AuNF-PEI-MIL-101(Cr) nanocomposites that act as the substrate material significantly increase the aptamer loading efficiency, further

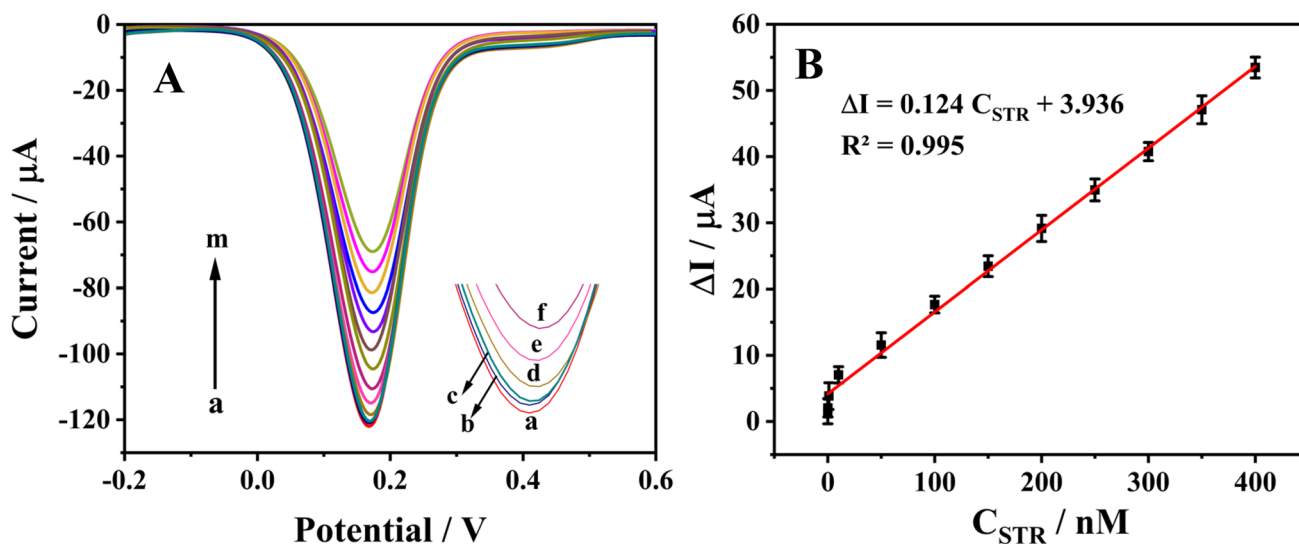


**Fig. 5** **A** DPV curves of the electrochemical aptasensor for the detection of different concentrations of STR (from a to m: 0, 0.01, 0.1, 1, 10, 50, 100, 150, 200, 250, 300, 350, and 400 nM). **B** The linear rela-

tionship between  $\Delta I$  and the concentration of STR ( $\Delta I = I - I_0$ , where  $I_0$  represents the blank DPV peak current)

enhancing the sensitivity of the aptasensor. (ii) The STR aptamer, as recognition molecules, is not only easy to synthesize, preserve, and modify, but also has good specificity and high affinity for the target STR.

### Reproducibility, Stability, and Selectivity of the Electrochemical Sensing Method

In order to investigate the reproducibility of the aptasensor, six independently prepared aptamer/AuNF-PEI-MIL-101(Cr)/GEs were used to detect STR of 50 nM at room temperature. As shown in Fig. S1A, there was little difference in the DPV peaks current, and the relative standard deviation (RSD) was less than 2%, suggesting that the aptasensor has good reproducibility.

In addition, the storage stability of the proposed aptasensor was also studied. The STR/aptamer/AuNF-PEI-MIL-101(Cr)/GEs were stored in a refrigerator (4°C) for 21 days (The concentration of STR is 50 nM), followed by periodical measurement of the current signals of electrodes. As shown in Fig. S1B, the current signals slowly declined with increasing storage time. After 21 days, the current signals of STR/aptamer/AuNF-PEI-MIL-101(Cr)/GEs were 94.29% of their original current signals. It indicated that the electrochemical aptasensor possessed desirable stability.

The specificity of an aptasensor is an essential indicator to achieve accurate detection. Eight other antibiotics, including neomycin, oxytetracycline, tetracycline, penicillin, chloramphenicol, kanamycin, erythromycin, and cephalexin hydrate, were selected as interfering antibiotics for detection. The concentration of STR and interfering substances was 100 nM. As shown in Fig. S1C, compared with the blank, only STR caused a distinct change in current signals, whereas other antibiotics showed no clear change. The selectivity factor ( $\alpha$ ) was calculated from the following formula (Amouzadeh Tabrizi and Acedo 2022; Zhang et al. 2018a, b).

$$\alpha = \Delta I_{STR} / \Delta I_{IS} \quad (2)$$

where  $\Delta I_{STR}$  and  $\Delta I_{IS}$  are the changes in the response of the aptasensor in the absence and presence of 100 nM STR and 100 nM interfering substances, respectively. The value of  $\alpha$  for neomycin, oxytetracycline, tetracycline, penicillin, chloramphenicol, kanamycin, erythromycin, and cephalexin hydrate were 8.58, 10.76, 11.26, 5.25, 8.25, 11.63 and 20.47, respectively. The values of  $\alpha$  were higher than 1, proving that the selectivity of the developed aptasensor to STR was high.

### The STR Detection in Real Samples

In order to demonstrate the applicability of this method in actual analysis, a standard addition method was used for STR detection in cow, sheep, and goat milk samples. The cow, sheep,

and goat milk samples containing 1 nM, 10 nM, and 50 nM spiked STR were prepared according to the procedure described in the “Samples preparation” section. The recovery was calculated as the ratio of the found STR concentration to the actually added concentration of STR, which was presented as the recovery percentage (%). As shown in Table S2, the recovery data obtained were in the range of 96.0–109.4% and the relative standard deviations were between 0.55 and 1.41%. To verify the reliability of the aptasensor, the commercially available ELISA kit as a standard method was employed to verify above results. Paired *t*-test was used to determine the difference between the two methods, and statistical analysis showed no significant difference between the methods ( $P > 0.05$ ). The results suggested that this aptasensor showed great application potential for rapid detection of STR in real food samples.

### Conclusions

A label-free electrochemical aptasensor based on AuNF-PEI-MIL-101(Cr) nanocomposites was successfully fabricated for the detection of STR. The AuNF-PEI-MIL-101(Cr) nanocomposites effectively enhanced the active electrode surface area and conductivity, resulting in an outstanding performance of the designed aptasensor. Under optimum conditions, the aptasensor showed a wide linear range (0.01–300 nM), a low detection limit (0.003 nM), and good reproducibility, stability, and specificity. In addition, the aptasensor could be successfully utilized for STR determination in the milk samples with satisfactory results. Given the properties mentioned above, this method can serve as a novel detection platform for other antibiotics by choosing appropriate aptamer sequences and possesses great potential in food safety.

**Supplementary Information** The online version contains supplementary material available at <https://doi.org/10.1007/s12161-023-02446-z>.

**Author Contribution** All authors contributed to the study conception and design. Yuanyuan Hui wrote the main manuscript. Material preparation, data collection, and analysis were performed by Yuanyuan Hui, Haishuai Peng, Ding Yang, and Weizhe Wang. Linqiang Li, Aiqing Zhao, and Bini Wang revised it critically for important intellectual content. Bini Wang provided financial support. All authors read and approved the final manuscript.

**Funding** This study was supported by the Science and Technology Program of Xi'an City (20NYF0018) and the Supported by the Fundamental Research Funds for the Central Universities (2021CBLY007).

**Data Availability** The authors declare that the data supporting the findings of this study are available within the article.

### Declarations

**Competing interests** The authors declare no competing interests.

**Ethics Approval** This article does not contain any studies with human participants or animals performed by any of the authors.

**Conflict of Interest** Yuanyuan Hui declares that he has no conflict. Haishuai Peng declares that he has no conflict of interest. Linqiang Li declares that he has no conflict of interest. Aiqing Zhao declares that he has no conflict of interest. Ding Yang declares that he has no conflict of interest. Weizhe Wang declares that he has no conflict of interest. Bini Wang declares that he has no conflict of interest.

## References

- Amouzadeh Tabrizi M, Acedo P (2022) An electrochemical immunosensor for the determination of procalcitonin using the gold-graphene interdigitated electrode. *Biosensors* 12(10):771. <https://doi.org/10.3390/bios12100771>
- Bayazit S, Yildiz M, Aşçi Y, Şahin M, Eglence S, Salam M (2017) Rapid adsorptive removal of naphthalene from water using graphene nanoplatelet/MIL-101 (Cr) nanocomposite. *J Alloy Compd* 701:740–749. <https://doi.org/10.1016/j.jallcom.2017.01.111>
- Biswas S, Lan Q, Xie Y, Sun X, Wang Y (2021) Label-free electrochemical immunosensor for ultrasensitive detection of carbohydrate antigen 125 based on antibody-immobilized biocompatible mof-808/cnt. *ACS Appl Mater Inter* 13(2):3295–3302. <https://doi.org/10.1021/acsami.0c14946>
- Chen B, Zhang H, Lin B, Ge J, Qiu L (2012) Determination of streptomycin residue in cucumber and chinese cabbage by high-performance liquid chromatography with postcolumn derivatization and fluorometric detection. *J Aoac Int* 95:523–527. <https://doi.org/10.5740/jaoacint.10-316>
- Chen Y, Liu Z, Guo L, Cao J, Zhou J, Zuo J, Bai L (2019) A sandwich-type electrochemical aptasensor for Mycobacterium tuberculosis MPT64 antigen detection using C60NPs decorated N-CNTs/GO nanocomposite coupled with conductive PEI-functionalized metal-organic framework. *Biomaterials* 216:119253. <https://doi.org/10.1016/j.biomaterials.2019.119253>
- Cheng M, Lai C, Liu Y, Zeng G, Huang D, Zhang C, Qin L, Hu L, Zhou C, Xiong W (2018) Metal-organic frameworks for highly efficient heterogeneous Fenton-like catalysis. *Coordin Chem Rev* 368:80–92. <https://doi.org/10.1016/j.ccr.2018.04.012>
- Cheng Y, Barpaga D, Soltis J, Shuththanandan V, Chatterjee S (2020) Metal-organic framework based microfluidic impedance sensor platform for ultrasensitive detection of perfluorooctanesulfonate. *ACS Appl Mater Inter* 12:10503–10514. <https://doi.org/10.1021/acsami.9b22445>
- De Carvalho RC, Betts AJ, Cassidy JF (2020) Diclofenac determination using CeO<sub>2</sub> nanoparticle modified screen-printed electrodes – a study of background correction. *Microchem J* 158:105258. <https://doi.org/10.1016/j.microc.2020.105258>
- Duan Y, Wang N, Huang Z, Dai H, Xu L, Sun S, Ma H, Lin M (2019) Electrochemical endotoxin aptasensor based on a metal-organic framework labeled analytical platform. *Mat Sci Eng C-Mater* 108:110501. <https://doi.org/10.1016/j.msec.2019.110501>
- Gzde A, Pekiardmc U (2020) An electrochemical sandwich-type aptasensor for determination of lipocalin-2 based on graphene oxide/polymer composite and gold nanoparticles - sciencedirect. *Talanta* 210:120666. <https://doi.org/10.1016/j.talanta.2019.120666>
- Hai G, Wang H (2022) Theoretical studies of metal-organic frameworks: calculation methods and applications in catalysis, gas separation, and energy storage. *Coordin Chem Rev* 469:214670. <https://doi.org/10.1016/j.ccr.2022.214670>
- He B, Wang S (2021) An electrochemical aptasensor based on PEI-C<sub>3</sub>N<sub>4</sub>/AuNWs for determination of chloramphenicol via exonuclease-assisted signal amplification. *Microchim Acta* 188:22
- Ho T, Chan C, Chan KH, Wang Y, Lin J, Chang C, Chang C (2013) Development of a novel bead-based 96-well filtration plate competitive immunoassay for the detection of gentamycin. *Biosens Bioelectron* 49(15):126–132. <https://doi.org/10.1016/j.bios.2013.04.027>
- Huang Q, Lin X, Chen D, Tong X (2022) Carbon dots/alpha-Fe<sub>2</sub>O<sub>3</sub>-Fe<sub>3</sub>O<sub>4</sub> nanocomposite: Efficient synthesis and application as a novel electrochemical aptasensor for the ultrasensitive determination of aflatoxin B<sub>1</sub>. *Food Chem* 373:131145. <https://doi.org/10.1016/j.foodchem.2021.131415>
- Hui Y, Peng H, Zhang F, Zhang L, Liu Y, Zhao A, Jia R, Wang B, Song Y (2022) A novel electrochemical aptasensor based on layer-by-layer assembly of DNA-Au@Ag conjugates for rapid detection of aflatoxin M<sub>1</sub> in milk samples. *J Dairy Sci* 105(3):1966–1977. <https://doi.org/10.3168/jds.2021-20931>
- Kaufmann A, Butcher P, Maden K (2012) Determination of aminoglycoside residues by liquid chromatography and tandem mass spectrometry in a variety of matrices. *Anal Chim Acta* 711:46–53. <https://doi.org/10.1016/j.aca.2011.10.042>
- Lu Q, Zhang J, Liu X, Wu Y, Yuan R, Chen S (2014) Enhanced electrochemiluminescence sensor for detecting dopamine based on gold nanoflower@graphitic carbon nitride polymer nanosheet-polyaniline hybrids. *Analyst* 139(24):6556–6562. <https://doi.org/10.1039/c4an01595a>
- Lu M, Deng Y, Yi L, Lv J, Wang J (2018) Graphene aerogel-metal-organic framework-based electrochemical method for simultaneous detection of multiple heavy metal ions. *Anal Chem* 91(1):888–895. <https://doi.org/10.1021/acs.analchem.8b03764>
- Luo Y, Tian X, Yong D, Chen Q, Huang Y, Feng D, Ai C, Mi Y (2020) A photoelectrochemical aptasensor for the sensitive detection of streptomycin based on a TiO<sub>2</sub>/BiOI/BiOBr heterostructure. *Anal Chim Acta* 1115:33–40. <https://doi.org/10.1016/j.aca.2020.04.021>
- Mehmandoust M, Erk N, Naser M, Soyak M (2023) Molecularly imprinted polymer film loaded on the metal-organic framework with improved performance using stabilized gold-doped graphite carbon nitride nanosheets for the single-step detection of Fenamiphos. *Food Chem* 404:134627. <https://doi.org/10.1016/j.foodchem.2022.134627>
- Meng X, Gu H, Yi H, He Y, Chen Y, Sun W (2020) Sensitive detection of streptomycin in milk using a hybrid signal enhancement strategy of MOF-based bio-bar code and target recycling. *Anal Chim Acta* 1125:1–7. <https://doi.org/10.1016/j.aca.2020.05.041>
- Pourreza A, Askari S, Rashidi A, Seif A, Kooti M (2019) Highly efficient so<sub>2</sub> ag-functionalized mil-101(Cr) for adsorptive desulfurization of the gas stream: experimental and dft study. *Chem Eng J* 363:73. <https://doi.org/10.1016/j.cej.2019.01.133>
- Shen C, Wu S, Meng Q (2021) Construction of portable drinking water device using an agricultural biomass-derived material of polyethylenimine-grafted-corn cob. *Food Control* 130:108375
- Sun R, Lv R, Li Y, Du T, Chen L, Zhang Y, Zhang X, Zhang L, Ma H, Sun H, Qi Y (2023) Simple and sensitive electrochemical detection of sunset yellow and Sudan I in food based on AuNPs/Zr-MOF-Graphene. *Food Control* 145:109491. <https://doi.org/10.1016/j.foodcont.2022.109491>
- Suresh K, Matzger AJ (2019) Enhanced drug delivery by dissolution of amorphous drug encapsulated in a water unstable metal-organic framework (mof). *Angew Chem Int Edit* 58(47):16790–16794. <https://doi.org/10.1002/anie.201907652>
- Taghdisi S, Danesh N, Nameghi M, Ramezani M, Abnous K (2016) A label-free fluorescent aptasensor for selective and sensitive detection of streptomycin in milk and blood serum. *Food Chem* 203:145–149. <https://doi.org/10.1016/j.foodchem.2016.02.017>

- Thakur H, Kaur N, Sareen D, Prabhakar N (2017) Electrochemical determination of m. tuberculosis antigen based on poly(3,4-ethylenedioxythiophene) and functionalized carbon nanotubes hybrid platform. *Talanta* 171:115–123. <https://doi.org/10.1016/j.foodchem.2016.02.017>
- Vanbruijnsvoort M, Ottink S, Jonker K, Deboer E (2004) Determination of streptomycin and dihydrostreptomycin in milk and honey by liquid chromatography with tandem mass spectrometry. *J Chromatogr A* 1058(1–2):137–142. <https://doi.org/10.1016/j.chroma.2004.07.101>
- Villalonga A, Sánchez A, Vilela D, Mayol B, Martínez-Ruiz P, Villalonga R (2022) Electrochemical aptasensor based on anisotropically modified (Janus-type) gold nanoparticles for determination of C-reactive protein. *Microchim Acta* 189(8):309. <https://doi.org/10.1007/s00604-022-05420-4>
- Wan J, Li Y, Jiang Y, Lin L, Yin Y (2021) Silver-doped MIL-101(Cr) for rapid and effective capture of iodide in water environment: exploration on adsorption mechanism. *J Radioanal Nucl Ch* 328:1041–1054. <https://doi.org/10.1016/j.chroma.2004.07.101>
- Wang Y, Wang L, Chen H, Hu X, Ma S (2016) Fabrication of highly sensitive and stable hydroxylamine electrochemical sensor based on gold nanoparticles and metal–metalloporphyrin framework modified electrode. *ACS Appl Mater Inter* 8(28):18173–18181. <https://doi.org/10.1021/acsami.6b04819>
- Xin Q, Ouyang J, Liu T, Li Z, Li Z, Liu Y, Wang S, Wu H, Jiang Z, Cao X (2015) Enhanced interfacial interaction and CO<sub>2</sub> separation performance of mixed matrix membrane by incorporating polyethylenimine-decorated metal-organic frameworks. *ACS Appl Mater Inter* 7(2):1065–1077. <https://doi.org/10.1021/am504742q>
- Yao J, Yue T, Huang C, Wang H (2021) A magnified aptamer fluorescence sensor based on the metal organic frameworks adsorbed dna with enzyme catalysis amplification for ultra-sensitive determination of atp and its logic gate operation. *Bioorg Chem* 114:105020. <https://doi.org/10.1016/j.bioorg.2021.105020>
- Yin J, Guo W, Qin X, Zhao J, Pei M, Ding F (2017) A sensitive electrochemical aptasensor for highly specific detection of streptomycin based on the porous carbon nanorods and multifunctional graphene nanocomposites for signal amplification. *Sensor Actuat B-Chem* 241:151–159. <https://doi.org/10.1016/j.snb.2016.10.062>
- Yuan N, Gong X, Han B (2021) Hydrophobic fluororous metal-organic framework nano-adsorbent for removal of hazardous wastes from water. *ACS Appl Nano Mater* 4(2):1576–1585. <https://doi.org/10.1021/acsanm.0c03050>
- Zhang L, Wang G, Xiong C, Zheng L, He J, Ding Y, Lu H, Zhang G, Cho K, Qiu L (2018a) Chirality detection of amino acid enantiomers by organic electrochemical transistor. *Biosens Bioelectron* 105:121–128. <https://doi.org/10.1016/j.bios.2018.01.035>
- Zhang S, Piepers S, Shan R, Cai L, Mao S, Zou J, Ali T, De Vlieghe S, Han B (2018b) Phenotypic and genotypic characterization of antimicrobial resistance profiles in *Streptococcus dysgalactiae* isolated from bovine clinical mastitis in 5 provinces of China. *J Dairy Sci* 101:3344–3355. <https://doi.org/10.3168/jds.2017-14031>
- Zhang F, Niu T, Wu F, Wu L, Wang G, Li J (2021) Highly oriented MIL-101(Cr) continuous films grown on carbon cloth as efficient polysulfide barrier for lithium-sulfur batteries. *Electrochim Acta* 392:139028. <https://doi.org/10.1016/j.electacta.2021.139028>
- Zhao W, Wei J, Sun M, Liu X, Zhang Q, Zong C et al (2016) Colorimetric detection of Cu<sup>2+</sup> by surface coordination complexes of polyethyleneimine-capped au nanoparticles. *Sensor Actuat B-Chem* 223(411–416):411–416. <https://doi.org/10.1016/j.snb.2015.09.119>
- Zhou N, Wang J, Zhang J, Li C, Tian Y, Wang J (2013) Selection and identification of streptomycin-specific single-stranded dna aptamers and the application in the detection of streptomycin in honey. *Talanta* 108:109–116. <https://doi.org/10.1016/j.talanta.2013.01.064>
- Zhou Y, Huang X, Zhang W, Ji Y, Chen R, Xiong Y (2017) Multi-branched gold nanoflower-embedded iron porphyrin for colorimetric immunosensor. *Biosens Bioelectron* 102:9–16. <https://doi.org/10.1016/j.bios.2017.10.046>
- Zhu Q, Li H, Sun X, Han Z, Sun J, He H (2021) Rational incorporation of covalent organic framework/carbon nanotube (COF/CNT) composites for electrochemical aptasensing of ultra-trace atrazine. *J Mater Chem A* 9(25):8043–8050
- European Commission (2010) Commission regulation (EU) No 37/2010 of December 2009 on pharmacologically active substances and their classification regarding maximum residue limits in foodstuffs of animal origin.
- Mehmandoust M, Erk E E, Soylak M, Erk N, Karimi F (2022) Metal–organic framework based electrochemical immunosensor for label-free detection of glial fibrillary acidic protein as a biomarker. *Ind Eng Chem Res* acs.iecr.2c01445. <https://doi.org/10.1021/acs.iecr.2c01445>

**Publisher's Note** Springer Nature remains neutral with regard to jurisdictional claims in published maps and institutional affiliations.

Springer Nature or its licensor (e.g. a society or other partner) holds exclusive rights to this article under a publishing agreement with the author(s) or other rightsholder(s); author self-archiving of the accepted manuscript version of this article is solely governed by the terms of such publishing agreement and applicable law.